JOURNAL OF GEOPHYSICAL RESEARCH, VOL. 98, NO. A11, PAGES 19,455–19,464, NOVEMBER 1, 1993

Birkeland Currents in the Plasma Sheet

NIKOLAI A. TSYGANENKO[1] AND DAVID P. STERN

Laboratory for Extraterrestrial Physics, NASA Goddard Space Flight Center, Greenbelt, Maryland

ZEREFŞAN KAYMAZ

Department of Atmospheric Sciences, University of California, Los Angeles

A search was conducted for the signatures of Birkeland currents in the Earth's magnetic tail, using observed values of B_x and B_y from large sets of spacecraft data. The data were binned by x and y for $-10 > x_{GSM} > -35$ and $|y_{GSM}| \leq 20R_E$ ($\leq 30R_E$ for $x_{GSM} \leq -25R_E$) and in each bin their distribution in the (B_x, B_y) plane was fitted by least squares to a piecewise linear function. That gave average x-y distributions of the flaring angle between $\mathbf{B}_{xy}$ and the x direction, as well as that angle's variation across the thickness of the plasma sheet. Angles obtained in the central plasma sheet differed from those derived near the lobe boundary. That is the expected signature if earthward or tailward Birkeland current sheets are embedded in the plasma sheet, and from this difference we derived the dawn-dusk profiles of the tail Birkeland currents for several x_{GSM} intervals. It was found that (1) the Birkeland currents have the sense of region 1 currents, when mapped to the ionosphere; (2) both the linear current density (kiloamperes/R_E) and the net magnitude of the field-aligned currents decrease rapidly down the tail; (3) the total Birkeland current at $x \approx -10R_E$ equals ≈500–700 kA, which is ~30% of the net region 1 current observed at ionospheric altitudes, in agreement with model mapping results; and (4) the B_z and B_y components of the interplanetary magnetic field influence the distribution of Birkeland currents in the tail.

1. INTRODUCTION

The origin of region 1 Birkeland currents has been one of the major problems of magnetospheric physics. These are the primary currents through which energy flows to the polar cap and to the rest of the circuit of Birkeland currents, yet the only part of their pattern which can be identified with certainty is its average intersection with the polar ionosphere [*Iijima and Potemra*, 1976*b*].

Several theories exist about the flow of region 1 currents far from Earth. Their origin is often ascribed to the low-latitude boundary layer (LLBL), for example, in Figure 1 of *Siscoe and Maynard* [1991], and it has also been suggested that they come down directly along open field lines [*Maltsev and Lyatsky*, 1975] or as a diversion of the Chapman-Ferraro current on the magnetopause [*Coroniti and Kennel*, 1973]. As shown below, the tracing of field lines from the ionospheric footpoints of region 1 on the dayside indeed leads to the vicinity of the magnetopause. A significant portion of region 1, however, is connected to the nightside of the auroral oval, and that part seems to come from the plasma sheet. It is the purpose of the present work to quantitatively study its spatial distribution.

The usual signature of field-aligned current sheets is a shear of the magnetic field, a rotation of **B**. That is how Birkeland currents were first identified in low-altitude Earth orbit [*Zmuda and Armstrong*, 1974] and that is also their expected signature in the geotail; the latter would be a rotation, as z changes, of the projection $\mathbf{B}_{xy}$ of the **B** vector into the x-y plane. If the j_x component dominates the Birkeland current density in the tail, the effect should be most pronounced in the B_y component. Such shears between **B** in the plasma sheet and the tail lobe were in fact reported by *Ohtani et al.* [1988] and *Candidi et al.* [1990], having the same sense as the one expected from currents with region 1 polarity.

The present study examines the distribution of such shears more thoroughly, using a large database of averaged magnetic observations from ISEE 1 and 2, from HEOS 1 and 2, and from spacecraft of the IMP series, in particular IMP 8. The shear is studied statistically through the variation of B_y, not with z but with B_x, which reduces error from tail flapping and from variations in the scale thickness of the plasma sheet. The average magnitude of the Birkeland current was mapped this way in 80 bins covering $-10 \geq x \geq -35$, $|y| \leq 30$. As a byproduct, the flaring of $\mathbf{B}_{xy}$ in that region was also mapped.

The polarity of the deduced currents was consistently that of region 1, but the total current involved was only a fraction of what Iijima and Potemra observed near Earth. Very little of the current came from the distant tail, on the contrary most of it seemed to originate in the earthward portion of the scanned region.

2. DATA ANALYSIS

Two data sets were used in this study, collected in two regions of the tail: the near-Earth region with $-25 \leq x_{GSM} \leq -10R_E$ and the middle tail with $-35 \leq x_{GSM} \leq -25R_E$. These data were previously examined and averaged, magnetopause crossings were identified and observations outside the magnetosphere were removed. The first set consisted of vector averages obtained by the IMP, HEOS, and ISEE missions during 1966–1981, used earlier in magnetospheric modeling [*Tsyganenko*, 1987, 1989; *Peredo et al.*, 1993]. The second consisted of 140,620 5-min vector averages con-

[1]On leave from Institute of Physics, University of St. Petersburg, St. Petersburg, Russia.

Paper number 93JA01922.
0148-0227/93/93JA-01922$05.00

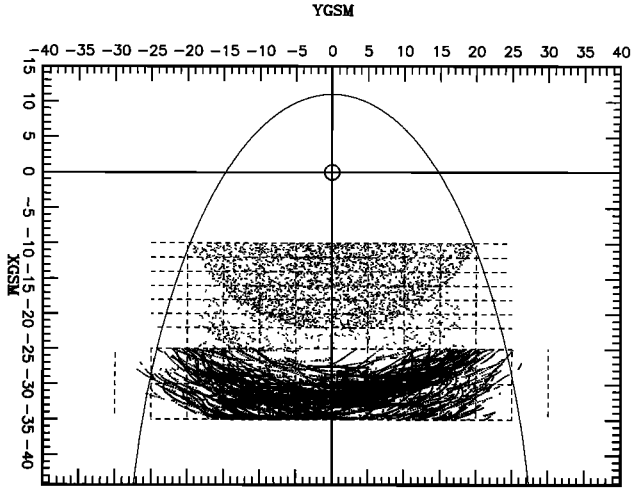

Fig. 1. Distribution of the data points used in this study, projected onto the equatorial plane. The division of the plasma sheet into bins of (x_{GSM}, y_{GSM}) is shown and a circular outer boundary with $R \approx 22R_E$ delineates the region covered by ISEE measurements. An average magnetopause boundary is included for reference.

structed from the higher resolution data of IMP 8 obtained during 1973–1988. Figure 1 shows the data point distribution for both tail regions as projected onto the equatorial plane.

To investigate the tail structure, the above data were divided into bins according to their values of x_{GSM} and y_{GSM} (from here on the subscripts will be omitted). In each bin we studied the variation of **B** across the thickness of the tail; one way of accomplishing this is by plotting the variation of the magnetic components as a function of $z' = z - z_s(x, y, \psi)$, where z_s is the value of z (at the same x and y) at the center of the plasma sheet, i.e., at the "neutral sheet." The function z_s depends on the dipole tilt ψ, and several model studies have derived approximate expressions for it [*Russell and Brody*, 1967; *Fairfield*, 1980; *Gosling et al.*, 1986; *Dandouras*, 1988; *Tsyganenko*, 1989; *Peredo and Stern*, 1991].

It turns out, however, that data ordered by z' still contain too much random scatter, due to variable magnetospheric and solar wind conditions which affect the tail. *Candidi et al.* [1990] overcame this difficulty by using plasma observations to classify magnetic measurements as belonging either to the plasma sheet or to the lobe, and then comparing **B** in the two regions.

Two problems arise when z' is used. The tail may flap in the north-south direction, displacing z_s by unknown amounts, and the tail's thickness may vary, narrowing or widening the profile of $B_y(z')$. As long as such narrowing and widening only changes the scale of the profile, however, the error it produces as well as the one due to flapping may be greatly reduced by using B_x as a proxy for z', i.e., by plotting B_y against B_x rather than against z'. That method is used here; a similar approach was used by *Bowling and Wolf* [1974]. All observations of the first data set were binned into $7 \times 8 = 56$ subsets corresponding to increments $\Delta x = 2R_E$ ($3R_E$ in the most distant bins) in the range $-25 \le x \le -10R_E$, and increments $\Delta y = 5R_E$ in the range $-20 \le y \le 20R_E$. Before observations were binned they were "filtered" by excluding points with $|z'| > 10R_E$, since such points were almost certain to be in the lobe and not in the plasma sheet. In this process a simple approximation was used for $z_s(x, y, \psi)$, independent of x, namely [*Tsyganenko*, 1989; *Peredo et al.*, 1993]

$$z_s = \left(R_H - G\frac{y^4}{y^4 + L_y^4}\right)\sin\psi \qquad (1)$$

where numerical values of the parameters were taken as $R_H = 9.6R_E$, $G = 6.6R_E$ and $L_y = 10R_E$, values derived for the average quiet state of the magnetosphere with $Kp = 2-$ to $2+$. The second data set was binned in the same way into 2×12 subsets with $\Delta x = \Delta y = 5R_E$, covering the region $-35 \le x \le -25R_E$ and $-30 \le y \le 30R_E$.

Figure 2 shows twelve distributions of B_y versus B_x obtained from the first data set for the near-Earth region. The left and right columns correspond to two ranges of x: $-14 \le x \le -12R_E$ and $-20 \le x \le -18R_E$, respectively, while the six rows, from top to bottom, correspond to six intervals of y, from $15 \le y \le 20R_E$ (dusk) to $-20 \le y \le -15R_E$ (dawn). The plots for $|y| \le 5R_E$ are omitted, because near the midnight meridian the features studied here become weak and are lost in the noise.

The first feature one notes in Figure 2 is the good correlation between B_x and B_y, displaying the expected proportionality near the middle of the sheet. Comparable plots of B_x against z' also show that correlation, but less distinctly, which supports our choice of B_x as a measure of the distance from the current sheet center.

It can also be seen from Figure 2 that the slopes of B_y against B_x are positive on the dawn side and negative on the dusk side, reflecting the flaring of the field lines away from the midnight meridian plane, due to the widening of the magnetopause in the antisunward direction [*Fairfield*, 1971, 1979]. The flaring angle can be easily calculated from the plots as $\alpha = \tan^{-1}(B_y/B_x)_{aver}$, which allows the distribution of the tail flaring angles in x and y to be derived.

One remarkable feature is conspicuous in almost all the plots, namely, the slope of the average variation of B_y versus is B_x is steepest in the middle portions of the graph, corresponding to $|B_x| \le 15$ nT. In other words, within a given (x, y) bin, the flaring angles are larger in the central plasma sheet than in the lobe. That is illustrated in Figure 3, which magnifies the distribution of B_y against B_x for $-14 \le x \le -12R_E$ and $-10 \le y \le -5R_E$ (also found in Figure 2, left column, third row from bottom) and adds trend lines fitted by least squares. The first line (solid) took into account only points with $|B_x| \ge B_c = 15$ nT, assumed to belong to the lobe and the plasma sheet boundary layer. The second line, shown broken, fitted all points to a piecewise continuous linear function:

$$\begin{aligned} B_y &= aB_x && |B_x| \le B_c \\ B_y &= aB_c' + b(B_x - B_c') && |B_x| \ge B_c \end{aligned} \qquad (2)$$

where $B_c' = B_c \,\mathrm{sign}\,(B_x)$ are the values of B_x at which the slope is discontinuous. We chose $B_c = 15$ nT for all the near-tail data sets, while the slopes a and b were fitted by least squares to the data point distribution. The fitting procedure shown for one bin in Figure 3 was repeated for the rest of the 56 bins covering the near-tail region. For each bin, the values of the tangents of the average local flaring angles were found by least squares for both the central plasma sheet

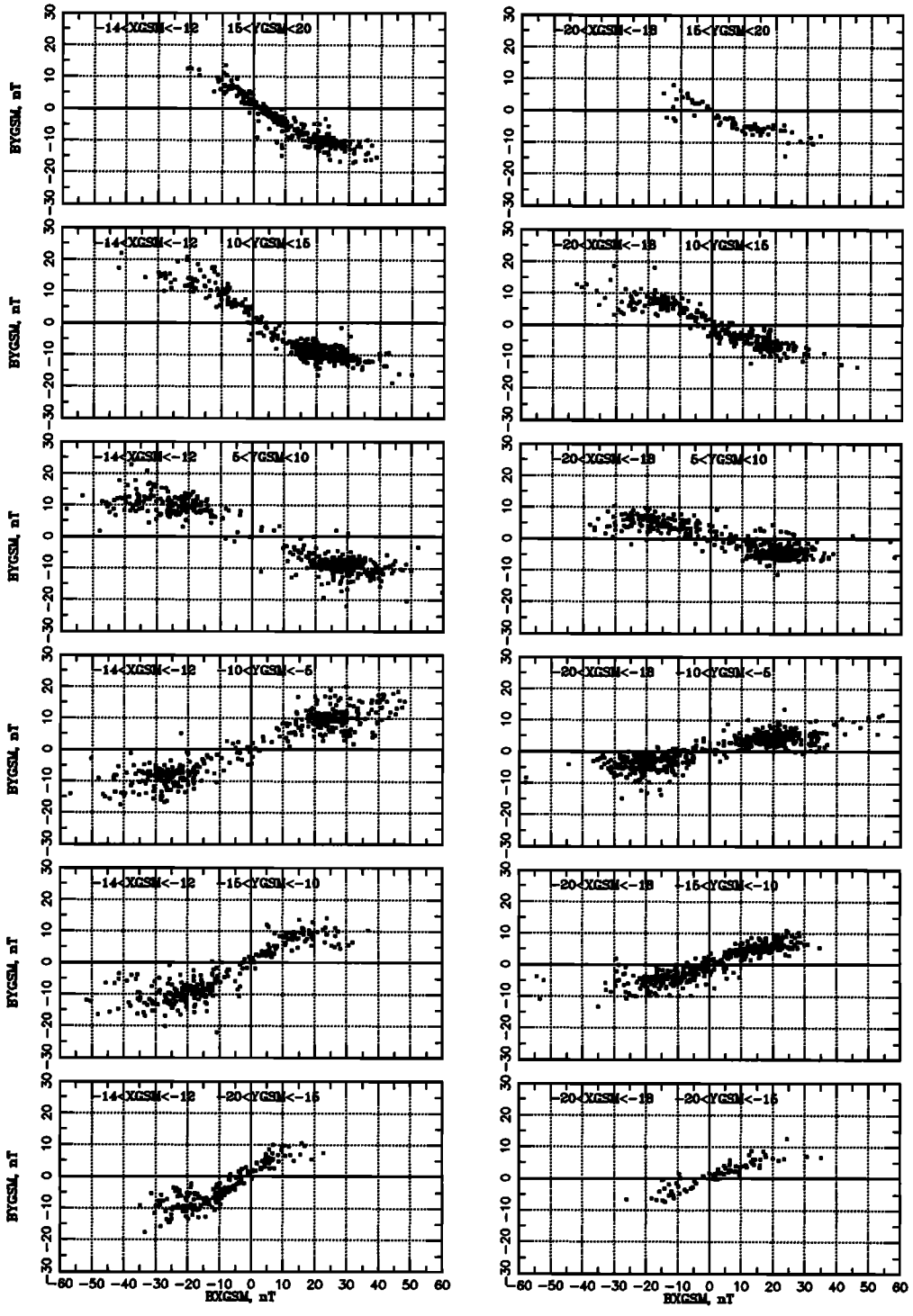

Fig. 2. The distribution of B_y against B_x plotted for 12 near-tail bins. Limits of x and y for each bin are shown in each panel. Note that a "saturation effect" for $|B_x| \geq 15$ nT is evident in almost all panels.

(CPS) and the tail lobe. The results are given in Figure 4, which shows the variation of both parameters across the tail.

Several features are clearly seen. First, near midnight the flaring angles vary linearly with y, while at larger $|y|$ they saturate, and in some bins even turn around and decrease again as the tail boundary is approached.

Second, the flaring effect decreases as one moves further down the tail. That is expected from the average observed shape of the tail boundary: the tail radius changes rapidly for $x \geq -20R_E$ [*Sibeck et al.*, 1991], but further tailward it tends to a limiting value $R_T \approx 25R_E$ [e.g., *Behannon*, 1970] and beyond the Moon's orbit it is almost constant and equal to R_T [*Slavin et al.*, 1985].

Third, as already noted above, the flaring angles are everywhere larger in the CPS than in the lobes. We believe this to be an indication of field-aligned currents flowing in the outer plasma sheet (or the plasma sheet boundary layer) and producing a shear between the lobe and CPS field lines, as

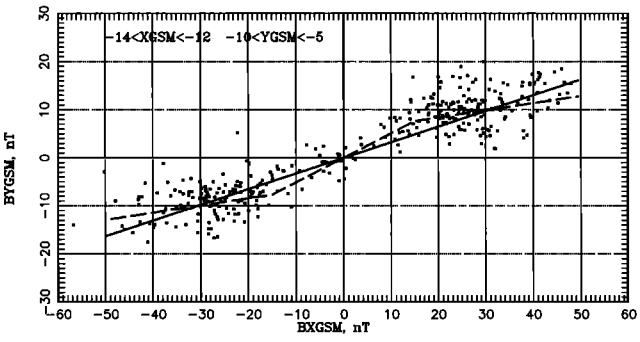

Fig. 3. Illustrating the least squares fitting of the distribution of B_y against B_x. The solid line is obtained by fitting points with $|B_x| \geq B_c = 15$ nT to a single line and hence gives the average flaring angle in the lobes and the plasma sheet boundary layer region. The broken line is a piecewise fit to all of data points: the slope a of its middle part equals the tangent of the average flaring angle inside the central plasma sheet. The slope b of the outer segments is smaller than a, which indicates the existence of a region 1 Birkeland current (see text).

found by *Candidi et al.* [1990]. This will be discussed in more detail below.

The analysis was repeated with 5-min averaged **B** vectors, measured by the IMP 8 magnetometer in the more distant tail region and binned in two ranges of x. The results are shown in Figure 5, which uses the same format as Figure 2, and in the last two panels of Figure 4. Qualitatively, the results resemble those obtained in the near tail. However, the absolute values of the flaring angles are smaller, as is the magnitude of the magnetic shear between the CPS and the lobe. Figure 6 displays the entire family of unit vectors $\mathbf{B}_{xy}/B_{xy}$ in the (x, y) plane, showing the overall distribution of the average flaring angles in the CPS (thin bars) and in the tail lobes (thick bars), obtained from fitting the near and middle tail data by least squares.

3. Discussion

The families of plots of B_y versus B_x shown in Figures 2 and 5 contain enough information for a quantitative study of Birkeland currents in the plasma sheet. Let us start with the general expression for the field-aligned current density:

$$j_\parallel = \frac{\mathbf{j}\cdot\mathbf{B}}{B} = \frac{c}{4\pi B}\left[B_x\left(\frac{\partial B_z}{\partial y} - \frac{\partial B_y}{\partial z}\right) + B_y\left(\frac{\partial B_x}{\partial z} - \frac{\partial B_z}{\partial x}\right) + B_z\left(\frac{\partial B_y}{\partial x} - \frac{\partial B_x}{\partial y}\right)\right] \quad (3)$$

Within the plasma sheet the derivatives $\partial/\partial x$ and $\partial/\partial y$ are much smaller than $\partial/\partial z$. Also, we assume that the B_x component varies monotonically across the plasma sheet, and therefore instead of z we can use B_x as an independent variable for measuring the distance from the center of the plasma sheet. With $d/dz = (dB_x/dz)(d/dB_x)$, we obtain from (3)

$$j_\parallel \approx \frac{c}{4\pi B} B_x \frac{dB_x}{dz}\left[\frac{B_y}{B_x} - \frac{dB_y}{dB_x}\right] \quad (4)$$

In the central plasma sheet B_y is proportional to B_x and hence $j_\parallel \approx 0$ there. However, as soon as $|B_x|$ exceeds the "critical" value B_c, the bracketed factor in (4) is no longer zero, and provided $dB_x/dz \neq 0$, (4) yields a nonzero field-aligned current density. If the slope in the inner part of the plot of B_y versus B_x is larger than in the outer part (as is the case in almost all the plots of Figures 2 and 5), then the sense of the Birkeland current in the plasma sheet boundary layer, as given by (4), is that of region 1: earthward in the dawn sector and tailward at dusk.

As we increase the z distance from the center of the plasma sheet, we enter the tail lobe region where $dB_x/dz \approx 0$ and hence $j_\parallel$ again becomes very small. Therefore Birkeland currents are localized in a transition region which can include the plasma sheet boundary layer. Note that according to (4), an additional enhancement of the PSBL field-aligned current can be caused by a local increase in the factor dB_x/dz produced by a dawn-dusk diamagnetic current, an effect often observed as a sudden increase (decrease) of the magnetic field when a spacecraft exits (enters) the plasma sheet. This effect however is not evident when B_x is used in place of z, as was done in Figures 2 and 5. Additional information on the average variation of **B** and **j** across the plasma sheet, as deduced from magnetometer data, is given by the early study of *Bowling and Wolf* [1974]; a more recent one, based on a statistical study which also included plasma measurements, was performed by *Kistler et al.* [1993].

Let us evaluate the linear current density $J_\parallel$ (in amperes per meter) of the net field-aligned current. To do that, we have to integrate (4) across the current-carrying region from $z = z_c$ to $z = z_m$, where the inner boundary position, z_c, corresponds to $B_x = B_c$ and where z_m is on the boundary of the lobe, on which $B = B_m$. We thus have

$$J_\parallel = \frac{c}{4\pi}\int_{z_c}^{z_m} \frac{B_x}{B}\frac{dB_x}{dz}\left[\frac{B_y}{B_x} - \frac{dB_y}{dB_x}\right] dz \quad (5)$$

which, after inserting the linear approximation (2) for B_y and assuming that $|B_x| \approx B$ for $z > z_c$, leads to a simple estimate of the net Birkeland current per unit distance in the dawn-dusk direction

$$J_\parallel = (c/4\pi)B_c(a - b)\ \ln\ (B_m/B_c) \quad (6)$$

The parameters entering (6), B_m, B_c, a, and b, can be evaluated by fitting them to the distributions shown in Figures 2 and 5. There exists some uncertainty as to the estimate of the average tail lobe field B_m: the average values should be somewhat smaller than the maximal values of $|B_x|$ taken from the data distributions. However, even significant errors in estimating B_m will be greatly reduced by the logarithmic dependence in (6). As a crude estimate we can take $B_m/B_c \approx 2 - 3$, based on visual inspection of the plots in Figures 2 and 5, as well as on values of B_m found at 20–40 R_E [*Fairfield*, 1979] and at larger distance [*Slavin et al.*, 1985]. Therefore the logarithmic factor can be assumed to equal unity, and with B_c in nanoteslas the final formula for the field-aligned current density simplifies to

$$J_\parallel \approx 5.07B_c(a - b)\ \text{kAmp}/R_E, \quad (7)$$

Figure 7 shows the variation of $J_\parallel$ along the dawn-dusk direction for eleven intervals of x. All plots show field-aligned current distributions with the polarity of the region 1 current system, flowing tailward for $y > 0$ and sunward for

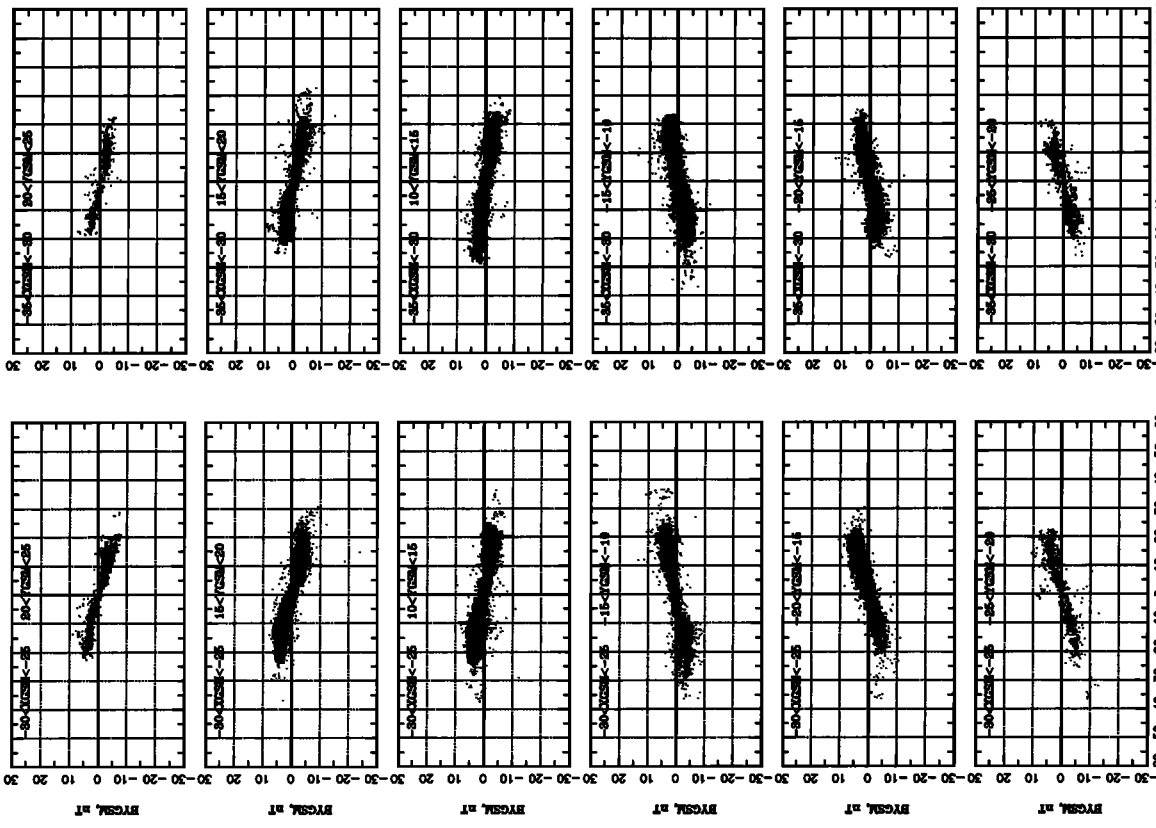

Fig. 5. Distribution of B_y against B_x plotted for 12 x-y bins in the middle tail. The data were taken by the IMP 8 magnetometer between $x = -25R_E$ and $x = -35R_E$ and have a higher time resolution (5 min) than the near-tail data of Figure 2.

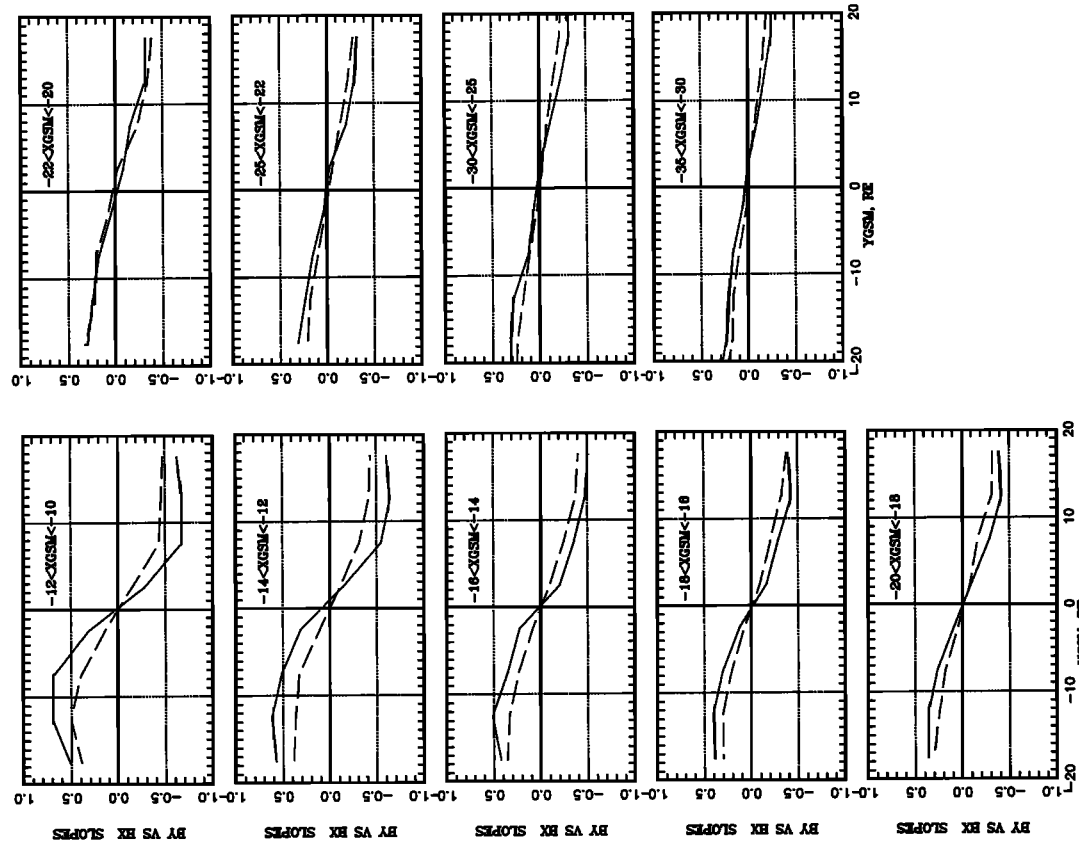

Fig. 4. The dawn-dusk variation of the average slopes of B_y plotted against B_x, approximately equal to the tangent of the field line flaring angles, for nine intervals of x, seven from the ISEE-IMP-HEOS data set at $x \geq -25R_E$, the other two from the IMP 8 data. Solid lines correspond to the central plasma sheet, dashed lines to the tail lobes. Note that the flaring angles in the CPS are everywhere larger than in the corresponding lobe plots.

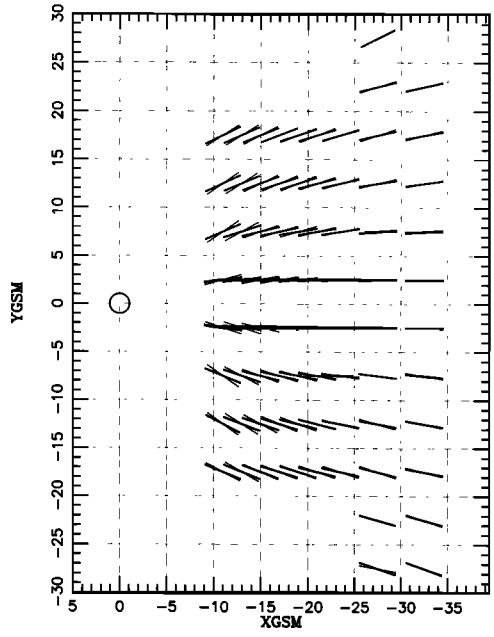

Fig. 6. An overall x-y view of the average magnetic field flaring pattern in the near-equatorial tail. Each of the unit vectors shows a bin-averaged orientation of the magnetic field in the central plasma sheet (thin bars) and lobe (thick bars). Note a gradual decrease of the rotation angles between the two with increasing distance down the tail.

$y < 0$. In spite of large fluctuations in the original distributions (Figures 2 and 5) all the plots in Figure 7 reveal a well-ordered variation of $J_\parallel$ with y and x. That variation has the following features:

1. The field-aligned currents reverse their direction near the midnight meridian and can be roughly approximated by an odd function of y. The departure from ideal mirror symmetry may be taken as a measure of the random noise level inherent in this analysis: noise is present, but it does not qualitatively affect the results.

2. The net Birkeland current flowing between midnight and the dawn (or dusk) magnetopause, evaluated by integrating the plotted functions between $y = 0$ and $y = 20R_E$, or $y = -20R_E$ equals 500–700 kAmp, with the larger figure obtained from the analysis of 1-min averages, noted further below. The highest estimate is found in the first plot, the x bin nearest to the Earth, and that is to be expected since any bin must also carry all the currents originating tailward from it. Comparing that value with the average estimate of the net region 1 current at the ionospheric level (e.g., *Iijima and Potemra* [1978]) which amounts to $J_I = 2 \times 10^6$ A, we have to conclude that only ≈25–30% of this current originates tailward of $x = -10R_E$.

That agrees with the results of *Iijima and Potemra* [1976*a*, *b*], as shown in Figure 8. The figure shows a family of 73 field lines starting from the average ionospheric trace of quiet-time Birkeland currents [*Iijima and Potemra*, 1976*b*, Figure 6], traced with the T89 model [*Tsyganenko*, 1989] at the $Kp = 2$ level. The model used new revised coefficients based on the combined IMP-HEOS-ISEE data set [*Peredo et al.*, 1993] which do not suffer from the problems noted by *Donovan et al.* [1992]. The model's magnetopause was traced by following a bundle of field lines that passed close to the dayside neutral point, and its equatorial cross section is drawn as a dashed line.

The footpoints of each pair of neighboring field lines differ in magnetic local time (MLT) by 10 min, and lines corresponding to integral values of the MLT are drawn heavier. The field line which crosses the equator at the broken line $x = -10R_E$ reaches the ionosphere around MLT = 19.5 hours, and Figure 3*a* of *Iijima and Potemra* [1976*a*] suggests that field lines arriving at Earth further nightward indeed carry ~30% of the total region 1 current, as was found here.

3. As can be observed in Figure 7, the net field-aligned current at IMP 8 distances is much smaller than at $x = -12R_E$. This suggests that most region 1 currents arise relatively close to Earth and rather little current originates at great distances (e.g., at a distant neutral line). The rapid decrease of the field-aligned currents down the tail observed in Figure 7 also suggests another reason why the tail Birkeland currents were not detected in the study by *Fairfield* [1979]: that work used data collected between 20 and 33 R_E, where the field-aligned currents are much weaker than in the near tail. See also *Candidi et al.* [1990] and note that those authors based their study on ISEE data taken at closer distances, where the shear effect is larger.

Another conspicuous feature is that the peak current magnitudes in the nearest x bin occur at $y = \pm 8R_E$ rather than closer to the tail flanks as might be expected from Figure 8. A possible reason could be that the current density is the sum of a smooth profile rising toward larger values of $|y|$ and a contribution by the substorm current wedge, which may peak closer to $|y| = 8$ and which also has the polarity of region 1 (we thank T. Potemra for suggesting this explanation). The peaking is much sharper when only observations with interplanetary magnetic field (IMF) $B_z < -1$ nT are used (Figure 9, below), during which time the expected contribution by substorm is larger than average.

The data used in the main region of this study ($-10 > x > -25R_E$) were all 15–30 min averages. To determine whether such averaging smeared out the effect, we repeated the calculation using 1-min average magnetic field data taken by ISEE 1 and 2 during the same 4-year period, and obtained essentially the same shape of the profiles. The absolute intensity of the Birkeland currents however turned out to be somewhat higher (by 20–50%); this will be further discussed in a future paper.

The next point concerns the IMF dependence of the tail's Birkeland currents. As shown by *Bythrow and Potemra* [1983], there exists a high correlation between the total Birkeland current observed at ionospheric altitudes and the estimate $VB \sin^2 \Theta/2$ of the merging electric field, where V is the solar wind velocity, B the intensity of the IMF, and Θ the angle between $\hat{z}$ and x-y component of the IMF **B**. If the Birkeland currents of the tail are the same as the ones observed at low altitude, they should also display a positive correlation with southward IMF. To verify this, we derived plots of $J_\parallel$ versus y, similar to the ones of Figure 7, for two subsets of the near-tail data corresponding to IMF $B_z > +1$ nT and IMF $B_z < -1$ nT. The results are shown in Figure 9 for the nearest bins of the near-tail data ($-12 < x < -10R_E$, solid line) and the most distant ones ($-25 < x < -22R_E$, dashed line). As expected, Birkeland currents are approximately twice as large with negative IMF B_z as they are for positive IMF B_z. In both cases the field aligned

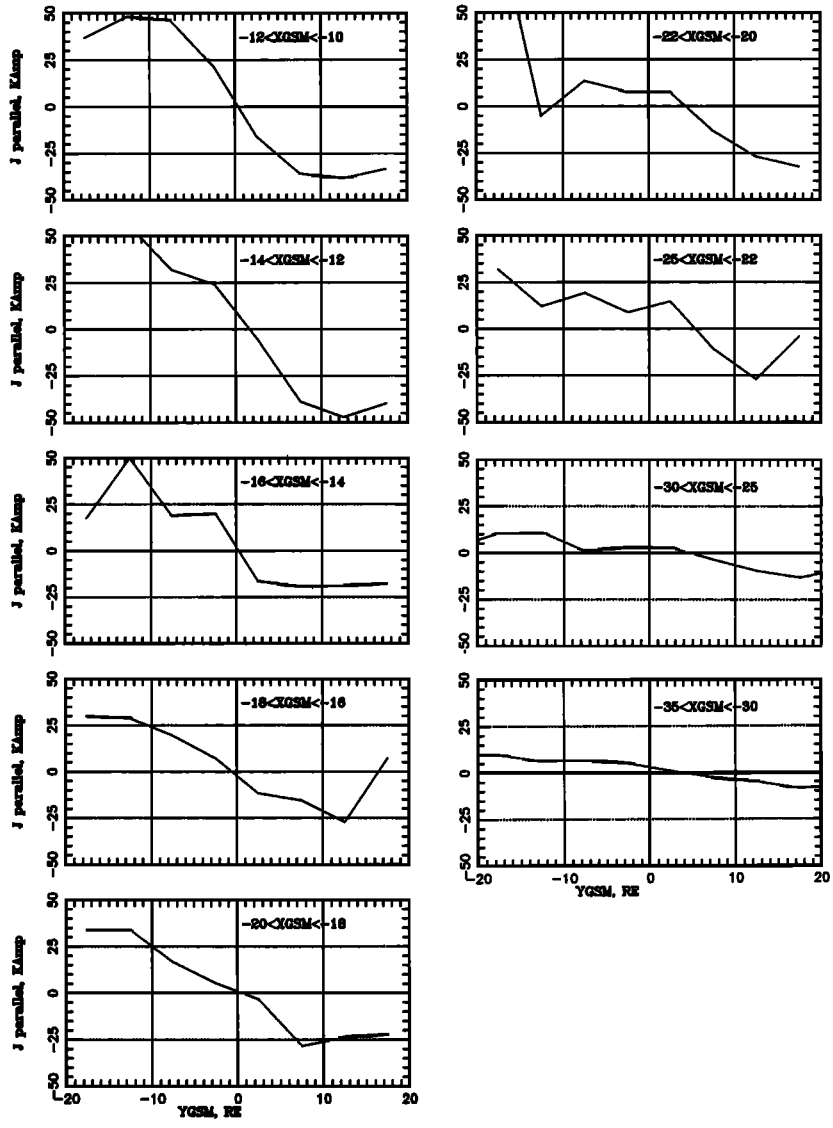

Fig. 7. The dawn-dusk variation of the Birkeland current for nine intervals of x in the near tail, obtained from the best fit values of the plot slopes of B_y versus B_x and equation (6). Note the gradual decrease of the currents with increasing distance down the tail, which also suggests a good fit between the ISEE-IMP-HEOS results (first seven panels) and those of IMP 8 (last two).

currents are again much weaker in the most distant x bin that in the nearest one. Note that the profiles are fairly symmetric about the midnight meridian plane.

The next pair of plots (Figure 10) uses the same format to show the effects of the polarity of IMF B_y on the tail's field-aligned currents. It is clearly seen that for positive (negative) IMF B_y the Birkeland currents are somewhat stronger on the duskside (dawnside). Ideally, the two plots should be mirror images of each other, and the departure from symmetry gives a measure of the variability of the results. *Lui* [1984] and *Sergeev* [1987] reported an additional feature of the magnetotail field's response to IMF B_y, namely an enhanced degree of penetration by B_y into the plasma sheet, in comparison with the lobe region. We could in principle check out this effect by allowing Birkeland currents to have different magnitudes and/or polarities in the northern and southern plasma sheet boundary layers. To

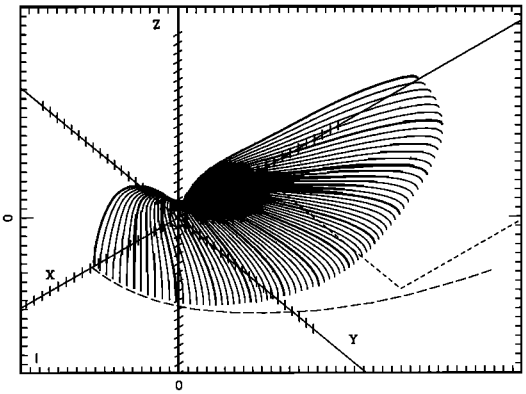

Fig. 8. Field lines traced from the average footpoints of region 1 currents, using a modified T89 model, at 10-min intervals of magnetic local time. Dashed lines in the equatorial plane outline the magnetopause and the boundary of the region studied here.

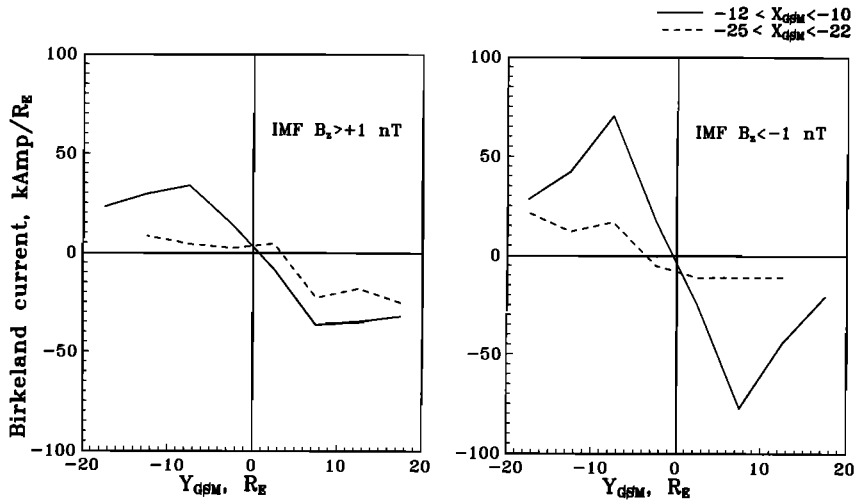

Fig. 9. The dawn-dusk variation of the Birkeland current in the nearest (solid line) and most distant (dashed line) x coordinate interval of the inner tail, for (left) IMF $B_z > +1$ nT and (right) IMF $B_z < -1$ nT.

allow our fitting functions to represent this effect, it would be necessary to introduce an additional term in (2), allowing the fitting function to be shifted along the B_y axis and also allowing different slopes for $B_x < -B_c$ and $B_x > B_c$. However, such a modification would increase the number of free parameters from 2 to 4, and in view of the relatively small amount of data (especially near the flanks) and the large scatter of individual points, this analysis was not pursued any further.

With regard to the effects of IMF B_z, one may ask how much does B_z affect the flaring of the tail's field lines in the x-y plane. Figure 11 shows the average ratio $\langle B_y/B_x \rangle$ obtained for the x bin nearest to Earth, plotted against y in the central plasma sheet (solid line) and in the tail lobe (dashed line), for two IMF B_z polarities and the same x intervals as the ones used in Figures 9 and 10. An obvious conclusion is that field line flaring in the CPS is significantly increased during southward IMF B_z, while almost no effect exists in the lobes. Therefore, if any change in the flaring pattern is associated with the reconnection-induced increase of the tail lobe flux, it is more likely to be observed in the x-z plane. We believe the effect seen here is entirely due to the buildup of Birkeland currents.

4. SUMMARY

This study set out to map the distribution of field-aligned currents in the tail. The expected signature of such currents is a magnetic shear, a variation of the $\mathbf{B}_{xy}$ component of the field with distance from the equatorial surface.

Such shear was studied statistically using a large data set of averaged observations by IMP, HEOS, and ISEE spacecraft at $-10 > x_{GSM} > -25R_E$ and by IMP 8 at $-25 > x_{GSM} > -35R_E$. The B_x component is used to gauge distance from the equator and the B_y component is plotted against it; because the data come from many different magnetospheric conditions, the points of the B_y-B_x plots display considerable scatter and the average shears, extracted by least squares fitting, may still be somewhat inaccurate.

All Birkeland currents inferred here have the polarity of region 1 and are expected to link up with the pattern of

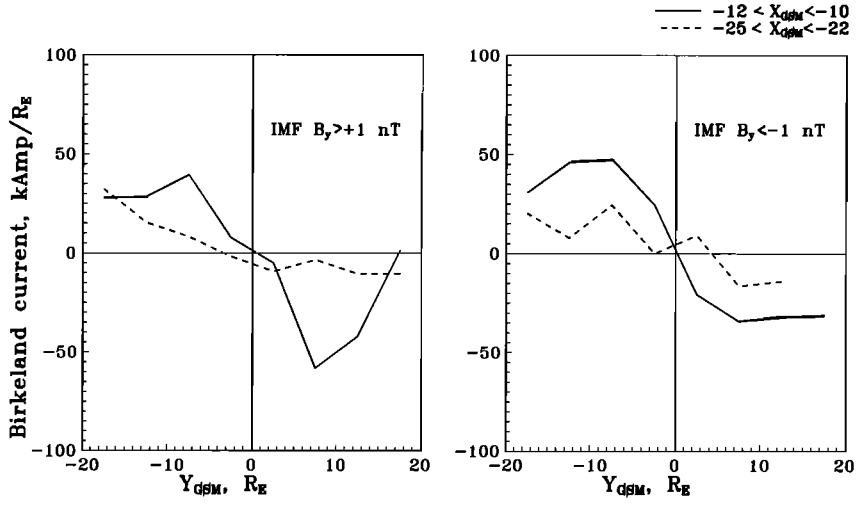

Fig. 10. Similar to Figure 8, for (left) IMF $B_y > +1$ nT and (right) IMF $B_y < -1$ nT.

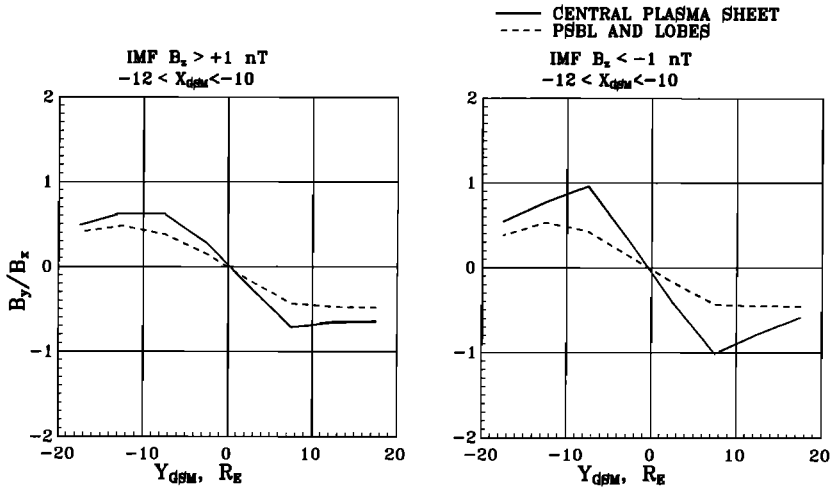

Fig. 11. Illustrating the effects of IMF B_z upon field line flaring angles in the central plasma sheet (solid line) and plasma sheet boundary layer (dashed line), for $-12 \leq x \leq -10R_E$. The left panel is for IMF $B_z > +1$ nT, the right one for IMF $B_z < -1$ nT.

region 1 currents observed near the Earth [*Iijima and Potemra*, 1976*a*, *b*]. The fact that such currents were traced back to the plasma sheet agrees with results of field-line mapping. Most of the current inferred in this study originates fairly close to Earth, and its intensity decreases by a factor 4–5 between $x \approx -10R_E$ and $x \approx -35R_E$. The total current flow found in the tail was only ~30% of the region 1 current observed near Earth, since it only corresponded to currents originating on the nightside of the polar cap, at MLT between 19.5 and 4.5 hours.

The mapping of the Iijima-Potemra pattern to the tail leads one to expect (see Figure 8) that as one moves earthward, the peak of the linear current density (kiloamperes/R_E) moves gradually toward the flank, reaching approximately $|y| = 15R_E$ at the near-Earth edge of the studied region. The actual peak in the data is closer to $|y| = 10$, which might reflect an added contribution from the substorm wedge current, expected to peak at smaller $|y|$. We look forward to the upcoming Cluster mission to observe these currents not statistically but on individual passes; the steeply inclined Cluster orbit, cutting across the plasma sheet in the north-south direction, seems well-suited for such a study.

The average region 1 currents derived here were found to depend on the IMF. As expected, they are more intense with southward IMF B_z, and at such time may be expected to contain an appreciable contribution from the substorm wedge current. They also show clear dawn-dusk asymmetry effects in response to IMF B_y. In addition to the shears, we also derived the pattern of field line flaring in the x-y plane in the plasma sheet, expected to be an important input for modeling the magnetotail.

Acknowledgments. This work was done while one of us (N.A.T.) held a National Research Council-NASA/GSFC Research Associateship. We gratefully acknowledge discussions with George Siscoe and Tom Potemra.

The Editor thanks M. Candidi and R. Elphic for their assistance in evaluating this paper.

REFERENCES

Behannon, K. W., Geometry of the geomagnetic tail, *J. Geophys. Res.*, *75*, 743–753, 1970.

Bowling, S. B., and R. A. Wolf, The motion and magnetic structure of the plasma sheet near $30R_E$, *Planet. Space Sci.*, *22*, 673–686, 1974.

Bythrow, P. F., and T. A. Potemra, The relationship of total Birkeland currents to the merging electric field, *Geophys. Res. Lett.*, *10*, 573–576, 1983.

Candidi, M., S. Orsini, M. Stokholm, and R. Elphic, On the structure of the tail magnetic field, *J. Geophys. Res.*, *95*, 7929–7936, 1990.

Coroniti, F. V., and C. F. Kennel, Can the ionosphere regulate magnetospheric convection?, *J. Geophys. Res.*, *78*, 2837–2851, 1973.

Dandouras, J., On the average shape and position of the geomagnetic neutral sheet and its influence on plasma sheet statistical studies, *J. Geophys. Res.*, *93*, 7345–7353, 1988.

Donovan, E. F., G. Rostoker, and C. Y. Huang, Region of negative B_z in the Tsyganenko 1989 model neutral sheet, *J. Geophys. Res.*, *97*, 8697–8700, 1992.

Fairfield, D. H., Average and unusual locations of the Earth's magnetopause and bow shock, *J. Geophys. Res.*, *76*, 6700–6716, 1971.

Fairfield, D. H., On the average configuration of the geomagnetic tail, *J. Geophys. Res.*, *84*, 1950–1958, 1979.

Fairfield, D. H., A statistical determination of the shape and position of the geomagnetic neutral sheet, *J. Geophys. Res.*, *85*, 775–780, 1980.

Gosling, J. T., D. J. McComas, M. F. Thomsen, S. J. Bame, and C. T. Russell, The warped neutral sheet and plasma sheet in the near-Earth geomagnetic tail, *J. Geophys. Res.*, *91*, 7093–7099, 1986.

Iijima, T., and T. A. Potemra, The amplitude distribution of field-aligned currents at northern high latitudes observed by Triad, *J. Geophys. Res.*, *81*, 2165–2174, 1976*a*.

Iijima, T., and T. A. Potemra, Field-aligned currents in the dayside cusp observed by Triad, *J. Geophys. Res.*, *81*, 5771–5979, 1976*b*.

Iijima, T., and T. A. Potemra, Large-scale characteristics of field-aligned currents associated with substorms, *J. Geophys. Res.*, *83*, 599–615, 1978.

Kistler, L. M., W. Baumjohann, T. Nagai, and E. Möbius, Superposed epoch analysis of pressure and magnetic field configuration changes in the plasma sheet, *J. Geophys. Res.*, *98*, 9249–9258, 1993.

Lui, A. T. Y., Characteristics of the cross-tail current in the Earth's

magnetotail, in *Magnetospheric Currents*, *Geophys. Monogr. Ser.*, vol. 28, edited by T. A. Potemra, pp. 158–169, AGU, Washington, D. C., 1984.

Ohtani, S., S. Kokubun, R. C. Elphic, and C. T. Russell, Field-aligned current signatures in the near-tail region, 1, ISEE observations in the plasma sheet boundary layer, *J. Geophys. Res.*, *93*, 9709–9720, 1988.

Peredo, M., and D. P. Stern, On the position of the near-Earth neutral sheet: A comparison of magnetic model predictions with empirical formulas, *J. Geophys. Res.*, *96*, 19,521–19,524, 1991.

Peredo, M., D. P. Stern, and N. A. Tsyganenko, Are existing magnetospheric models excessively stretched?, *J. Geophys. Res.*, *98*, 15,343–15,354, 1993.

Russell, C. T., and K. I. Brody, Some remarks on the position and shape of the neutral sheet, *J. Geophys. Res.*, *72*, 6104–6106, 1967.

Sergeev, V. A., Penetration of the B_y-component of the interplanetary magnetic field (IMF) into the tail of the magnetosphere, *Geomagn. Aeron.*, (Engl. Trans.), *27*, 528–530, 1987.

Sibeck, D. G., R. E. Lopez, and E. C. Roelof, Solar wind control of the magnetopause shape, location, and motion, *J. Geophys. Res.*, *96*, 5489–5495, 1991.

Siscoe, G. L., and N. Maynard, Distributed two-dimensional region 1 and region 2 currents: Model results and data comparisons, *J. Geophys. Res.*, *96*, 21,071–21,085, 1991.

Slavin, J. A., E. J. Smith, D. G. Sibeck, D. N. Baker, R. D. Zwickl, and S.-I. Akasofu, An ISEE 3 study of average and substorm conditions in the distant magnetotail, *J. Geophys. Res.*, *90*, 10,875–10,895, 1985.

Tsyganenko, N. A., Global quantitative models of the geomagnetic field in the cislunar magnetosphere for different disturbance levels, *Planet. Space Sci.*, *35*, 1347–1358, 1987.

Tsyganenko, N. A., A model of the magnetospheric magnetic field with a warped tail current sheet, *Planet. Space Sci.*, *37*, 5–20, 1989.

Zmuda, A. J., and J. C. Armstrong, The diurnal flow pattern of field-aligned currents, *J. Geophys. Res.*, *79*, 4611–4619, 1974.

Z. Kaymaz, Department of Atmospheric Sciences, University of California, Los Angeles, CA 90024.

D. P. Stern and N. A. Tsyganenko, Laboratory for Extraterrestrial Physics, NASA Goddard Space Flight Center, Greenbelt, MD 20771.

(Received January 27, 1993;
revised May 17, 1993;
accepted June 25, 1993.)